Published in final edited form as:

Curr Biol. 2021 June 07; 31(11): 2274–2285.e5. doi:10.1016/j.cub.2021.03.024.

Homeostatic Synaptic Scaling Establishes the Specificity of an Associative Memory

Chi-Hong Wu[1,†], **Raul Ramos**[1,†], **Donald B Katz**[2], **Gina G Turrigiano**[1,*]

[1]Department of Biology, Brandeis University, Waltham, MA 02453, USA

[2]Department of Psychology, Brandeis University, Waltham, MA 02453, USA

SUMMARY

Correlation-based (Hebbian) forms of synaptic plasticity are crucial for the initial encoding of associative memories, but likely insufficient to enable the stable storage of multiple specific memories within neural circuits. Theoretical studies have suggested that homeostatic synaptic normalization rules provide an essential countervailing force that can stabilize and expand memory storage capacity. Although such homeostatic mechanisms have been identified and studied for decades, experimental evidence that they play an important role in associative memory is lacking. Here we show that synaptic scaling, a widely studied form of homeostatic synaptic plasticity that globally renormalizes synaptic strengths, is dispensable for initial associative memory formation but crucial for the establishment of memory specificity. We used conditioned taste aversion (CTA) learning, a form of associative learning that relies on Hebbian mechanisms within gustatory cortex (GC), to show that animals conditioned to avoid saccharin initially generalized this aversion to other novel tastants. Specificity of the aversion to saccharin emerged slowly over a time-course of many hours and was associated with synaptic scaling down of excitatory synapses onto conditioning-active neuronal ensembles within gustatory cortex. Blocking synaptic scaling down in the gustatory cortex enhanced the persistence of synaptic strength increases induced by conditioning and prolonged the duration of memory generalization. Taken together, these findings demonstrate that synaptic scaling is crucial for sculpting the specificity of an associative memory and suggest that the relative strengths of Hebbian and homeostatic plasticity can modulate the balance between stable memory formation and memory generalization.

eTOC Blurb

[*]**Author Contact:** Gina Turrigiano (turrigiano@brandeis.edu).
Lead Contact: Gina Turrigiano
[†]Co-First Authors

AUTHOR CONTRIBUTIONS

Conceptualization, C.H.W., R.R., D.B.K., & G.G.T.; Methodology, C.H.W., R.R., D.B.K., & G.G.T.; Investigation, C.H.W. & R.R.; Formal Analysis, C.H.W. & R.R.; Writing – Original Draft, C.H.W., R.R., & G.G.T.; Writing – Review and Editing, C.H.W., R.R., D.B.K., & G.G.T.; Funding Acquisition, R.R., D.B.K., & G.G.T.; Resources, D.B.K., & G.G.T.; Supervision, D.B.K., & G.G.T.

DECLARATION OF INTERESTS

The authors declare no competing interests.

Wu, Ramos et al. use conditioned taste aversion to demonstrate that homeostatic synaptic scaling sculpts the specificity of associative memory. Perturbation of synaptic scaling down in the gustatory cortex prolongs the duration of both generalized aversion and CTA-induced increases in synaptic strength in the conditioning-activated ensemble.

Keywords

Homeostatic Synaptic Plasticity; Synaptic Scaling; Gustatory Cortex; Conditioned Taste Aversion; Learning; Memory; Memory Generalization; Memory Specificity

INTRODUCTION

The full complement of cellular plasticity mechanisms that enable the encoding and maintenance of specific memories within neural circuits are incompletely understood. While Hebbian modification of synapses through long-term potentiation (LTP) is important for associative memory formation,[1–3] LTP is thought to be insufficient to faithfully encode memories due to its positive feedback nature, where stronger connections are more likely to undergo further strengthening.[4,5] Theoretical work has shown that such “fire together, wire together” Hebbian learning rules can lead to unconstrained and non-specific synaptic strengthening, which in turn is predicted to degrade memory storage.[4–8] This problem can be solved by introducing synaptic normalization rules that homeostatically constrain synaptic weights,[4] but although cellular plasticity mechanisms with the right properties to normalize synaptic weights have been identified and studied for decades,[9,10] experimental evidence that they play a critical role in associative memory is lacking. Here we show that synaptic scaling, a widely studied form of homeostatic synaptic plasticity that slowly renormalizes synaptic strengths,[11,12] is dispensable for the initial rapid formation of conditioned taste aversion (CTA) memory, but is crucial for the slower establishment of memory specificity.

Homeostatic synaptic scaling is a cell-autonomous, negative feedback mechanism that bidirectionally scales excitatory postsynaptic strengths to maintain neuronal activity within a set-point range.[9,12–14] It has long been hypothesized to stabilize neuronal activity in the face of learning-driven changes in synaptic strength.[10,11] However, while LTP is rapidly induced, [2,3] synaptic scaling unfolds over many hours,[10,13] suggesting that it cannot stabilize Hebbian plasticity on short timescales.[7] This temporal dissociation suggests that unopposed Hebbian plasticity during the early stage of associative memory formation might result in a memory that initially generalizes beyond the specific stimulus used for conditioning; by slowly renormalizing synaptic weights, synaptic scaling might then establish memory specificity over a time course of many hours. While the notion that memory specificity might gradually emerge as a result of the slow induction of synaptic scaling is compelling on theoretical grounds, this hypothesis has not been tested.

Here we asked how synaptic scaling shapes memory specificity in conditioned taste aversion (CTA) learning, a form of associative learning that relies on Hebbian plasticity within the gustatory cortex (GC).[15–19] We found that following CTA conditioning, animals transitioned from a generalized to a taste-specific aversion over a timescale of ~24 hours. Blocking

synaptic scaling in the gustatory cortex using viral manipulations prolonged this generalized aversion. Additionally, we found that when animals exhibited a generalized aversion, gustatory cortex neuronal ensembles active during conditioning were robustly reactivated by the novel tastant. Abolishing synaptic scaling led to a persistent increase in postsynaptic strengths onto neurons in these gustatory cortex conditioning-active ensembles, that correlated with the prolonged generalized aversion. Our work demonstrates that synaptic scaling down of synaptic strengths within gustatory cortex is important for sculpting the specificity of CTA memory, and that the homeostatic regulation of synaptic strengths is important for establishing the balance between stable memory formation and generalization.

RESULTS

CTA memory specificity emerges over a timescale of hours

CTA is a classic form of associative learning thought to be specific to the conditioned tastant,[20,21] yet it can generalize to other novel tastants.[22,23] This raised the possibility that the specificity of the aversive memory might emerge with time after conditioning. To investigate this, we used a CTA two-bottle test where animals choose between a tastant and water (Figure 1A); this standard CTA paradigm is sensitive to a range of aversion strengths.[16] Young Long-Evans rats (postnatal days p28-p32) of both sexes underwent CTA conditioning, where saccharin was paired with an intraperitoneal LiCl injection (0.15 M, Moderate CTA group) to induce transient gastric malaise. Male and female rats showed comparable CTA (as well as generalized aversion, see below) so data from both sexes were combined (Figure S1). A memory test with saccharin (CTA Test) 4 hours post-conditioning revealed a decrease in the taste preference score (consumption of saccharin/total consumption), indicating an aversion to saccharin in the Moderate CTA group compared to the Conditioned Stimulus Only control group (CS, no LiCl, Figure 1B), as expected.

To test for a generalized aversion (Gen. Test), we performed CTA as above, and 4 hours post-conditioning presented animals with a choice between water and NaCI, a novel tastant that is easily discriminated from saccharin.[24] This revealed that conditioning to saccharin also induced a significant aversion to NaCl (Figure 1C). This aversion was not a result of past tastant experience or LiCl-induced malaise, as no aversion was evident in the CS Only and Unconditioned Stimulus Only (US, LiCl) controls, respectively (Figure 1C). Thus, during the early stage of CTA-memory formation, animals exhibit an aversion that generalizes to a novel tastant. To determine how long this generalized aversion persists we next performed the Gen. Test at 24 hours post-conditioning. At this timepoint, Moderate CTA rats demonstrated no significant difference in taste preference score compared to CS Only controls (Figure 1D). These results indicate that, over a time course of many hours, CTA memory transitions from a non-specific generalized aversion to a memory that is specific to the conditioned stimulus.

The onset of memory specificity depends on the intensity of conditioning

Higher concentrations of LiCl enhance CTA strength,[25] and we wondered if this would prolong the duration of the generalized aversion. As opposed to the Moderate CTA group, which exhibits no generalized aversion after 24 hours, the Strong CTA group (0.30 M LiCl)

exhibited a persistent generalized aversion 24 hours post-conditioning (Figure 1D). This aversion was not a result of more substantial malaise induced by LiCl treatment, as the US Only (0.30 M) controls showed no generalized aversion (Figure 1D). Thus, stronger CTA conditioning prolonged the duration of the generalized aversion. These experiments reveal an interaction between the strength of conditioning and the onset of CTA memory specificity.

We wondered whether the generalized aversion induced by CTA conditioning would attenuate with repeated exposure. Indeed, while tastant preference in control groups did not change, the generalized aversion induced by Strong CTA reversed upon repeated exposure to NaCl, suggesting that the generalized aversion memory (like CTA itself)[26,27] is subject to reversal or extinction (Figures 1E–1G). There were no differences between any experimental conditions in tastant consumption during conditioning (Figures S2A–S2D). Animals in both moderate and strong conditioning groups demonstrated significant aversion to saccharin after generalized aversion testing, confirming the formation of CTA memory (Figures S2A,S2E and S2F). Notably, but not surprisingly, conditioning resulted in a floor effect across both moderate and strong CTA groups due to the sensitivity of the two-bottle choice test (see Bures et al., 1998 for an explanation of CTA methodology).[16] Together, these results demonstrate that the time course over which the specificity of CTA memory emerges is sensitive to the intensity of CTA conditioning.

Neurons in the gustatory cortex express homeostatic synaptic scaling

The many hours-long time course over which CTA memory specificity emerges is reminiscent of the slow time course of homeostatic forms of plasticity such as synaptic scaling.[9,13,28] This raises the interesting possibility that synaptic scaling might contribute to the establishment of memory specificity by slowly counteracting the effects of rapid unconstrained conditioning-associated Hebbian plasticity.[17,18] Synaptic scaling has been extensively studied in sensory cortices,[11,29,30] but whether neurons in gustatory cortex are capable of expressing synaptic scaling is an open question. To test this, we took a chemogenetic approach using hM4D(Gi) DREADDS (designer receptors exclusively activated by designer drugs)[31] to chronically inhibit pyramidal neurons in the gustatory cortex and probe for the induction of synaptic scaling. Long-Evans rats received unilateral virus injections of AAV9-CAMKIIa-hM4D(Gi)-mCherry into the gustatory cortex at p14 and after two weeks showed robust expression (Figure 2A). In slice recordings from injected animals, acute application of CNO onto hM4D(Gi)$^+$ neurons in gustatory cortex resulted in hyperpolarization and a decrease in evoked spiking (Figure S3), confirming the expression of hM4D(Gi). Using the protocol outlined in Figure 2B, animals were randomly assigned to the control (CNO$^-$) or CNO treatment (CNO$^+$) groups. The contralateral, uninjected hemisphere of both CNO conditions served as an additional hM4D(Gi)$^-$ control for non-specific effects of CNO. After 2 days of chronic inhibition via CNO injection, we prepared brain slices from the gustatory cortex and recorded glutamatergic miniature excitatory postsynaptic currents (mEPSCs) from mCherry$^+$ pyramidal neurons to probe for the global changes in postsynaptic strength that underlie the induction of synaptic scaling (Figures 2C and 2D). We found a significant increase in mEPSC amplitude in the inhibited (hM4D(Gi)$^+$ CNO$^+$) neurons compared to both control groups (Figure 2E) but no change in mEPSC

frequency (Figure 2F), as expected for classic synaptic scaling.[9,12] Analysis of the cumulative distribution function (CDF) of mEPSC amplitude from inhibited neurons revealed a significant shift towards higher amplitudes relative to control (hM4D(Gi)$^-$ CNO$^+$) (Figure 2G). To test whether mEPSC amplitude increased multiplicatively, as is characteristic of synaptic scaling,[9] we plotted ranked inhibited vs. ranked control amplitudes and fit a linear function to the data;[9,32] scaling the inhibited distribution down generated a distribution that was statistically indistinguishable from the control (Figure 2G). These results demonstrate that in response to activity perturbations, neurons in the gustatory cortex can homeostatically compensate through synaptic scaling.

Both synaptic scaling up and down are known to depend on C-terminal sequences on the GluA2 subunit of AMPA receptors,[13,28,33–35] and expression of the C-terminal fragment of GluA2 (the GluA2-Ctail) has been shown to block synaptic scaling in visual cortex pyramidal neurons.[28,33] To determine if synaptic scaling in gustatory cortex pyramidal neurons is similarly dependent on GluA2 interactions, we next used a viral vector to express the GluA2-Ctail in gustatory cortex. Rats received co-injections of AAV9-CAMKIIα-hM4D(Gi)-mCherry and either AAV2/1-GluA2-Ctail-GFP (GluA2-Ctail) or AAV2/1-GFP (Empty Vector) (Figure 2H), were treated with CNO as above, and then recordings were obtained from hM4D(Gi)$^+$ neurons ± the GluA2-Ctail (Figure 2I). This revealed that mEPSC amplitude was higher in inhibited neurons expressing the Empty Vector than in those expressing the GluA2-Ctail (Figure 2J), indicating that synaptic scaling in gustatory cortex relies on GluA2-Ctail interactions for its expression.

Perturbation of synaptic scaling prolongs CTA-induced generalized aversion

If synaptic scaling shapes the specificity of CTA memory by constraining runaway LTP, then blocking synaptic scaling should prolong the expression of the generalized aversion. To test this hypothesis, we bilaterally expressed either the GluA2-Ctail or Empty Vector in the gustatory cortex, subjected animals to moderate CTA conditioning, and then probed for a generalized aversion (Figures 3A, 3B top and 3B bottom left). Consistent with our previous dataset (Figure 1D); generalized aversion was gone 24 hours after conditioning in animals expressing Empty Vector (Figure 3C). In striking contrast, in animals expressing the GluA2-Ctail the generalized aversion was still present at this late time point (Figure 3C). Furthermore, this prolonged generalized aversion rapidly reversed after repeated exposure to NaCl (Figure 3F), while the same testing paradigm induced no change in taste preference in the Empty Vector group, where generalized aversion was absent (Figure 3E). We then conducted an unpaired reverse conditioning paradigm in which animals received saccharin six hours after LiCl injection (Figures S4A–S4C). In this paradigm animals were exposed to both tastant experience and LiCl-induced malaise, but no CTA was formed (Figure S4D). GluA2-Ctail expression did not alter the preference to novel NaCl 24 hours after reverse conditioning (Figure 3D), confirming that the effect of the GluA2-Ctail relies on the initial induction of associative memory.

Scaling up and down, as well as some forms of LTD, rely on GluA2-Ctail interactions.[13,28,33–35] To differentiate between them we next used a manipulation that blocks scaling down, but not scaling up or LTD (see discussion): expression of the PDZ1/2 domains of

PSD95 (PSD95-PDZ1/2).[36] An AAV vector expressing PSD95-PDZ1/2 was bilaterally injected into gustatory cortex (Figure 3B bottom right), and one week later we tested for generalized aversion as described above. As with the GluA2-Ctail, PSD95-PDZ1/2 expression significantly prolonged the generalized aversion (Figure 3C), and this reversed after repeated NaCl exposure (Figure 3G). This finding demonstrates that disruption of synaptic scaling down in gustatory cortex is sufficient to prevent the transition from a generalized to a specific aversion.

Finally, as a third means of blocking synaptic scaling we used a GluA2 phosphorylation mutant (Y876E) that disrupts protein-protein interactions critical for synaptic scaling.[37,38] We bilaterally injected a lentiviral vector expressing either GluA2-Y876E or wild-type GluA2 (GluA2-WT) under control of a CAMKIIα promoter, and one week later subjected rats to our generalized aversion paradigm. While expression of GluA2-WT did not affect memory specificity, GluA2-Y876E expression prolonged the generalized aversion, which reversed after repeated NaCl exposure (Figures S5A–S5C). None of these manipulations affected the consumption of saccharin during the conditioning trial, indicating these effects are not due to enhanced neophobia (Figures S5D and S5E). In all cases, rats were left with an associative aversion to saccharin after generalized aversion testing was complete, demonstrating that formation of CTA memory was not impaired by blockade of synaptic scaling (Figures S5F and S5G). Because the CAMKIIα promoter used for the GluA2-Y876E construct mainly drives expression in cortical excitatory neurons,[39] these results suggest that homeostatic plasticity onto excitatory neurons in gustatory cortex plays a crucial role in shaping stimulus specificity during CTA.

Conditioning-active gustatory cortex neuronal ensembles are reactivated during generalized aversion

A subset of neurons activated during conditioning will form the engram, an ensemble of neurons that is reactivated during memory retrieval and is important for the expression of the memory.[40] The generalized aversion presumably occurs because – after conditioning – a novel tastant (such as NaCl) can activate these same ensembles that encode the aversive memory. We therefore wondered whether, during generalized aversion, ensembles of neurons within gustatory cortex activated by NaCl might overlap more strongly with ensembles active during conditioning. To label conditioning-activated ensembles and track their reactivation, we virally expressed a Robust Activity Marking (RAM) system in gustatory cortex.[41] RAM consists of a tTA element driven by the synthetic activity-dependent promoter P_{RAM} and a TRE-dependent tdTomato marker; doxycycline prevents tTA from interacting with TRE, thereby inhibiting the expression of tdTomato. By removing doxycycline prior to conditioning and then restoring it afterwards, expression of tdTomato can be restricted to neurons active during conditioning. Conditioning induced robust expression of RAM within dysgranular/agranular regions of GC and in both superficial and deep layers (Figure S6D).

We next took advantage of our ability to manipulate the duration of generalized aversion by controlling the intensity of CTA: generalized aversion induced by moderate conditioning is gone by 48 hours, while that induced by strong conditioning persists at this time point

(Figures S6A and S6B). The longer interval between the conditioning trial and the generalization test ensures that doxycycline fully inhibits further expression of tdTomato. Animals first underwent moderate or strong conditioning, and 48 hours later were exposed to the novel tastant NaCl; endogenous expression of the immediate early gene c-FOS was used to label neurons activated by the NaCl exposure (Figure 4A). By comparing the degree to which a novel tastant reactivates the conditioning-active ensemble during moderate and strong CTA training, we can examine reactivation in the absence and presence of generalized aversion to NaCl (Figure 4B). The reactivation rate of RAM-positive neurons during NaCl exposure was significantly higher in the Strong CTA than in the Moderate CTA or the CS Only groups (Figure 4C). The distribution of RAM-positive neurons was similar among CS Only, Moderate CTA, and Strong CTA groups, consistent with previous reports that engram size remains constant despite changes in the strength of conditioning[42,43] (Figure 4D). Furthermore, the number of c-FOS-positive neurons in gustatory cortex was not significantly different across experimental groups, indicating that the expression of generalized aversion is not determined by the size of active neuronal ensembles during NaCl exposure (Figure 4E). We confirmed that the overlap between RAM-positive neurons and c-FOS-positive neurons was above chance level in all groups (Figure S6C). These results demonstrate that during the expression of generalized aversion, a novel tastant induces robust reactivation of the conditioning-active gustatory cortex ensemble.

Blocking synaptic scaling causes a persistent increase in synaptic strength onto CTA-active neuronal ensembles following CTA conditioning

Why is NaCl able to reactivate conditioning-active ensembles during generalized aversion? One possibility is that runaway Hebbian plasticity induced by associative conditioning[17,18] transiently increases excitatory synaptic strengths onto this ensemble, and thus enhances the ability of novel tastants to activate and recruit members of the ensemble. If so, then subsequent homeostatic scaling down of synaptic strengths might sculpt the specificity of CTA memory by renormalizing synaptic strengths and thus reducing excitability. This hypothesis predicts that synaptic strength onto conditioning-active ensembles should be potentiated when the generalized aversion is expressed and reduced again as the generalized aversion fades and memory specificity is established. To test this, we used RAM to label the conditioning-activated neuronal ensemble in the gustatory cortex (Figure 5A), and then prepared brain slices and recorded from RAM^+ ($tdTomato^+$) neurons (Figure 5B) 24 hours after Moderate or Strong CTA induction to compare synaptic strengths in the presence or absence of generalized aversion, respectively (Figure 5C). We found that mEPSC amplitudes were significantly larger in the Strong CTA condition compared to the Moderate CTA condition (Figure 5D). Moreover, mEPSC amplitudes onto RAM^+ cells in the Moderate CTA condition were similar to those from control, uninfected neurons (Figure 2E).

Next, we asked whether the decrease in excitatory synaptic strengths onto RAM+ neurons when generalized aversion is gone (the Moderate CTA condition) could be prevented by blocking synaptic scaling. Indeed, RAM^+ neurons in the Moderate CTA+GluA2-Ctail group had significantly higher mEPSC amplitudes and rightward-shifted amplitude distribution compared to RAM^+ neurons in the Moderate CTA condition alone (Figures 5D and 5E), and were not significantly different from the Strong CTA condition. Taken together these data

show that synaptic strengths onto conditioning-active ensembles are first potentiated and then homeostatically downscaled during Moderate CTA learning; blocking synaptic scaling in gustatory cortex keeps synaptic strengths onto these conditioning-activated ensembles potentiated, and prolongs the generalized aversion measured behaviorally (Figure 6).

DISCUSSION

An important role for synaptic normalization in memory encoding has long been hypothesized,[4,5] but exactly how synaptic normalization rules like synaptic scaling influence the formation and stability of associative memories is unknown. Here we used a conditioned taste aversion (CTA) paradigm, a form of associative learning that relies on Hebbian mechanisms within gustatory cortex, to show that the specificity of an aversive memory emerges slowly over a time course of many hours, and is associated with synaptic scaling down of excitatory synapses onto conditioning-active neuronal ensembles within gustatory cortex. Blocking synaptic scaling down in gustatory cortex enhanced the persistence of synaptic strength increases onto these conditioning-active ensembles, and prolonged the duration of memory generalization. Our data show that synaptic scaling plays a critical role in establishing the specificity of an associative memory, and raises the interesting possibility that the relative strengths of Hebbian and homeostatic plasticity can be tuned to control the degree to which an associative memory will be generalized to other stimuli.

Synaptic scaling plays a well-established role in the stabilization of activity within primary sensory cortex during experience-dependent plasticity.[14,29,32,44] The evidence that synaptic scaling is important for learning and memory is more circumstantial; while disruption of signaling pathways important for synaptic scaling can induce memory deficits,[45,46] whether, where, and when synaptic scaling might be induced during associative memory paradigms, and its precise role in memory formation, is unknown. A major advantage of the paradigm we establish here is that the initial rapid formation of CTA memory, which relies on Hebbian mechanisms including LTP[17,18] and LTD at basolateral amygdala (BLA) projections to GC, [19] is followed by a slower process that establishes the specificity of the memory, allowing us to temporally dissociate these two processes. We find that CTA produces a net potentiation of synapses onto conditioning-active ensembles in gustatory cortex during generalized aversion, and that these synapses then slowly undergo synaptic scaling down as the memory becomes specific. We note that this initial net potentiation is not inconsistent with the selective depression of specific inputs such as those from the BLA during CTA memory formation.[19] Interestingly, blocking synaptic scaling had no impact on initial CTA memory formation, which depends on NMDA-dependent plasticity;[17] this is consistent with the slow time course of synaptic scaling, which theoretical work suggests should not be able to fully constrain Hebbian plasticity in the short term.[7] Rather than limiting initial memory formation, our data show that synaptic scaling is important for controlling the slow transition from a generalized to a specific memory.

Prior to this study it was unknown whether synaptic scaling was expressed in gustatory cortex; to test this we used viral expression of inhibitory DREADDs to chronically inhibit excitatory neurons in GC. This paradigm induced robust multiplicative synaptic scaling that was dependent on GluA2-Ctail interactions, indicating that it shares key molecular features

with synaptic scaling in other cortical areas.[28,33,35] Some forms of long-term depression (LTD) also depend on GluA2-Ctail interactions,[47,48] and the GluA2-Ctail can interfere with memory processes thought to depend on LTD.[49–51] On the other hand LTD and scaling down rely on distinct domains of PSD95: the N-terminal PDZ1/2 domains of PSD95 are required for synaptic scaling down[36,52] while its C-terminal Src homology 3(SH3) and guanylate kinase (GK) domains are critical for induction of LTD.[53,54] The common feature of all three manipulations we used to behaviorally extend the CTA-induced generalized aversion is their ability to block synaptic scaling down. Taken together with our physiological demonstration that synapses were downscaled as CTA memory became specific, and that blocking this synaptic downscaling prolonged the behaviorally measured generalized aversion, these data strongly support the view that synaptic scaling is the critical cellular mechanism within gustatory cortex that establishes the specificity of CTA memory.

The prevailing view of associative memory formation is that a subset of neurons activated during conditioning will undergo enduring changes and become a memory engram.[40] Apart from enabling memory retrieval, subpopulations of these conditioning-active ensembles may also regulate the generalizability of memory.[55] In our CTA paradigm, we found that the conditioning-active GC neurons are robustly reactivated by a novel tastant only during behavioral states in which the animals exhibit a generalized aversion to that tastant. The degree of reactivation by the novel tastant is comparable to the rate of reactivation by specific memory recall observed in other learning paradigms.[56] More importantly, excitatory synaptic strengths onto these conditioning-active neurons directly correlated with the expression of generalized aversion, while preventing synaptic scaling down specifically in GC increased the duration of this postsynaptic enhancement and prolonged behavioral generalization. Thus, the temporal dynamics of synaptic changes onto these ensembles nicely matches the dynamics of learning-related behavioral changes during CTA.

Generalization is an important aspect of aversive memories for which the cellular mechanism was largely obscure.[57] Here we demonstrate that the duration of generalized aversion following CTA is controlled by a homeostatic process that renormalizes synaptic strengths onto conditioning-active cortical ensembles to establishes the tastant specificity of CTA. Our data are consistent with a model in which unopposed Hebbian plasticity[17,18] onto GC neurons is important for initial CTA memory formation and generalization, while subsequent homeostatic synaptic downscaling slowly restores excitability and sculpts memory specificity. The initial generalization of CTA enabled by slow homeostatic compensation might be ethologically useful, by encouraging caution toward novel foods in an environment where such foods have recently proven dangerous. Conversely, if left unchecked persistent generalization of aversive conditioning could become pathological, as in post-traumatic stress disorders.[57,58] Our data suggest that the degree of specificity of CTA memory is malleable and can be controlled by the relative strengths of Hebbian and homeostatic plasticity within gustatory cortex.

STAR METHODS

RESOURCE AVAILABILITY

Lead contact—Further information and requests for resources and reagents should be directed to the lead contact, Gina G. Turrigiano (turrigiano@brandeis.edu).

Materials availability—Plasmids generated in this study are available from Lead Contact upon request.

Data and code availability—All data generated in this study are included in the figures and supplemental figures. Custom MATLAB codes used for analyses of electrophysiology data can be found at github.com/BrianAndCary/papers/tree/master/bcary2020_paper/mini_FI_GUI

EXPERIMENTAL MODEL AND SUBJECT DETAILS

All experimental procedures were approved by Brandeis University Institutional University Animal Care and Use Committee and followed the National Institute of Health guideline for the Care and Use of Laboratory Animals. Young Long-Evans rats (p28-p34) were used in these experiments. Timed pregnant rats were obtained from Charles River Laboratories, and the progeny were maintained in Foster Biomedical Research Labs at Brandeis University. After weaning at post-natal day 21 (p21), littermates were individually housed in a humidity-and temperature-controlled environment and entrained to a 12 hour light-dark cycle (light phase from 7:00-7:00) with ad libitum access to food and water unless described otherwise. In all behavioral experiments, because there were no sex differences in taste preference during Gen. test (24 hours post-conditioning), rats of both sexes were randomly assigned to different experimental conditions. For experiments that required virus-mediated manipulations, virus surgery was performed on animals at p14, which allowed the construct to be fully expressed at the time of conditioning (~p28). The average infection rates for neurons in GC for GluA2-Ctail and PSD-PDZ1/2 were 35.5% and 26% respectively (n = 3 for each condition), calculated as GFP^+NeuN^+ cells / $NeuN^+$ cells (%). For all behavioral experiments, viral expression was confirmed post hoc by immunostaining and all animals with detectable bilateral expression in GC were included for analysis. All subjects selected for electrophysiology experiments were age matched to animals selected for behavioral experiments.

METHOD DETAILS

Viral vectors—The pAAV-CMV-GluA2-CT (GluA2-Ctail) and pAAV-CMV-PSD95-PDZ1/2 (PSD-PDZ1/2) plasmids were constructed by sub-cloning the coding sequences of the scaling blockers[33,36] into the pAAV-CMV-eGFP3 vector (Empty Vector). pAAV-RAM-dtTA-TRE-tdTomato was constructed by replacing GFP in pAAV-RAM-dtTA-TRE-GFP (Addgene: 84469) with the coding sequence of tdTomato. pAAV-CAMKIIα-hM4D(Gi)-mCherry was obtained from Addgene (50477). Lenti-CAMKIIα-GFP-GluA2-Y876E and Lenti-CAMKIIα-GFP-GluA2-WT were generated by subcloning coding sequences of full-length GluA2 into a pLenti-CAMKIIα-c1v1 vector. For *in vivo* applications, GluA2-Ctail, PSD-PDZ1/2, and Empty Vector were packaged in AAV2 serotype 1; RAM-dtTA-TRE-

tdTomato and hM4D(Gi)-mCherry were packaged in AAV2 serotype 9. All viruses were produced at Duke Viral Vector Core, except for the GluA2-Ctail, which was packaged at UPenn Viral Vector Core.

Virus surgery—Rats were anesthetized with a cocktail containing ketamine (70 mg/kg, intraperitoneally (i.p.)), xylazine hydrochloride (3.5 mg/kg), and acepromazine maleate (0.7 mg/kg), and placed onto a stereotaxic apparatus. The skull was exposed, and craniotomies were made above GC. For the behavior experiments (GluA2-Ctail, PSD-PDZ1/2, Empty Vector) and imaging (RAM), viruses (800 nl per hemisphere) were bilaterally microinjected into GC through a glass micropipette connected to a micromanipulator (Narishige, MO-10), at a rate of approximately 200 nl/min. To cover the whole GC, three injection sites were chosen for each hemisphere: anterior-posterior (AP) with reference to bregma: 1.0 mm, medial-lateral (ML): ±4.7 mm, dorsal-ventral (DV) with reference to the brain surface: −3.5 mm, −3.6 mm, −3.7 mm. To allow adequate diffusion of virus particles, the pipet remained in place for additional 5 minutes after injection and was slowly withdrawn from the site. For DREADDS experiments, hM4D(Gi)-mCherry (400 nl) was unilaterally injected into GC. To label conditioning-active neurons for electrophysiological experiments, either RAM alone (400 nl), or a cocktail containing RAM and GluA2-Ctail (1:1, 400 nl) were bilaterally infused.

Behavioral paradigm

Two-bottle paradigm: This CTA behavioral paradigm was adapted from a previous study[59] and modified for our experimental needs. After being transferred into individual home cages, rats were habituated to two bottles with *ad libitum* access to water for three days. The animals were then subjected to water restriction for an additional three days, during which the access to water was limited to two hours. On the fourth day of restriction, rats underwent CTA conditioning. They received two bottles that contained the conditioned stimulus (CS), saccharin (10 mM), for thirty minutes, followed by an intraperitoneal injection of the unconditioned stimulus (US), LiCl (for moderate conditioning, 0.15 M; for strong conditioning, 0.30 M, 1% Body Weight). For the CS Only group, rats received saccharin, and were injected with saline instead of LiCl. For the US Only group, rats were given two bottles of water during the conditioning trial, followed by an injection of LiCl. After the conditioning, rats underwent a retention interval of 4 or 24 hours until testing. For a two-bottle choice test, rats were given one bottle of tastant, counterbalanced by one bottle of water, for thirty minutes. The results were quantified using a tastant preference score (TPS):

$$TPS = \frac{total\ tastant\ consumed}{total\ consumed} \times 100$$

To test CTA (CTA test), saccharin (10 mM) was used as the tastant. To test generalized aversion (Gen. test), NaCl (150 mM) was used. To measure the attenuation and reversal of the generalized aversion, Gen. tests were conducted daily for three days. After Gen. testing was complete, rats were given a CTA test to ensure that the animals had indeed learned an aversion to the CS. All the consumption was documented throughout the paradigm to ensure that daily fluid intake was stable.

Reverse conditioning: The same two-bottle training paradigm was conducted with the following modification: on the day of conditioning, rats first received injection of LiCl (0.15 M), and six hours later, 30-minute access to saccharin. Gen tests were then conducted the next day to match the 24-hour retention interval.

Administration of clozapine N-oxide (CNO): Rats underwent surgery as described above and were individually housed at p21. At p27-p30, CNO (3 mg/kg) was intraperitoneally administered every 12 hours for 2 days. Animals assigned to the DREADDS-only group underwent virus injection, but CNO was replaced with saline during the drug administration. After the treatment, acute brain slices were collected for electrophysiological analysis.

Labeling of conditioning-active neurons: Customized chow containing low-dose doxycycline (40 ppm, ScottPharma) were added to the home cage one day before virus surgery, and rats were maintained on doxycycline throughout the training. The doxycycline-containing chow was replaced with regular chow one day before the conditioning trial to allow adequate RAM induction. Two hours after the conditioning trial, rats were placed back on a diet containing high-dose doxycycline (100 ppm, ScottPharma) to prevent further RAM activation. To test the reactivation of conditioning-active ensembles, rats underwent the training paradigm as described above, except that they were given NaCl for thirty minutes 48 hours after the conditioning trial. Ninety minutes after the exposure, the animals were sacrificed for further immunohistochemistry experiments. For the electrophysiological experiments, acute brain slices were collected 24 hours after the conditioning trial.

Immunohistochemistry—Animals were deeply anesthetized with isofluorane and perfused with 4% paraformaldehyde (PFA). Brains were extracted, post-fixed in 4% PFA for 48 hours, and then sliced on a vibrating microtome (Leica Vibratome VT 1200s). Coronal brain slices (50 μm) containing GC were collected serially and stored in PBS until staining. For immunostaining, 2 slices were selected from anterior, middle, and posterior GC (6 slices in total) from each animal. Floating slices were washed three times with PBS, preincubated with blocking buffer (5% goat serum/3% BSA/0.3% Triton X-100 in PBS) at room temperature for 2 hours, and then incubated with primary antibodies diluted in blocking buffer at 4°C overnight. To verify expression of scaling blockers, chicken anti-GFP (1:1000, Aves Labs) and mouse anti-NeuN (1:500, MAB-377, Millipore) were used. To verify expression of hM4D(Gi), we used rat anti-mCherry (1:1000, ThermoFisher) and mouse anti-NeuN (1:500, MAB-377, Millipore). To label the reactivation of conditioning-active ensembles, mouse anti-RFP (1:1000, Rockland) and rabbit anti-cFOS (1:200, 9F6, Cell Signaling Technology) were used. On the next day, slices were first washed thoroughly with PBS 5 times, and then incubated with Alexa-conjugated secondary antibodies diluted in PBS containing 5% goat serum and 3% BSA at room temperature for 3 hours (goat anti-chicken Alexa-488, goat anti-mouse Alexa-594, goat anti-rat Alexa-594, goat anti-mouse Alexa-555, and goat anti-rabbit Alexa-647, 1:400, Thermo-Fisher). After 3 more washes with PBS, slices were either directly mounted onto the slides and cover slipped using DAPI-Fluoromount-G mounting medium (SouthernBiotech), or counterstained with Hoechst stain (1:1000, ThermoFisher) for 20 minutes before mounting with Fluoromount-G medium (SouthernBiotech).

Image acquisition and analysis—Images were acquired on a laser-scanning confocal microscope (Zeiss LSM880) using ZEN Black acquisition software (Zeiss). The boundaries of GC were manually determined based on the Paxinos and Watson rat brain atlas.[60] Images were obtained using tile scan under a 20× objective, with frame size of 512 × 512. For all experiments, acquisition settings including laser power, gain/offset and pinhole size were kept consistent. To quantify reactivation of conditioning-active ensembles, image tiles were first subjected to maximum intensity projection and stitch functions using ZEN Black, then analyzed using ImageJ/FIJI software (NIH, US). Images from each channel were background-subtracted using the rolling ball function, and then thresholded to outline RAM$^+$, c-FOS$^+$, and DAPI$^+$ cells. The rostral-to-caudal distribution of RAM$^+$ neurons varied slightly due to the efficacy of virus spread, but we found that RAM was most highly expressed in the middle GC in all experimental groups and had posterior spread in most cases. For each animal, 3 consecutive hemispheres that showed highest RAM expression were included for quantification. ROI of the same size (2 mm^2) was drawn to include all layers within dysgranular and agranular GC for all hemispheres across experimental groups; the average numbers of RAM$^+$, c-FOS$^+$, and DAPI$^+$ cells from all hemispheres were quantified using particle analysis function, and the reactivation rate was calculated as follows:

$$Reactivation(\%) = \frac{RAM^+cells}{RAM^+c-FOS^+cells} \times 100$$

The number of double-labeled cells compared with the chance level was also calculated to ensure that the reactivation was not due to random overlap:[61]

$$Chance = \frac{RAM^+cells}{DAPI^+cells} \times \frac{c-FOS^+cells}{DAPI^+cells}$$
$$Overlap = \frac{RAM^+c-FOS^+cells}{DAPI^+cells}$$
$$Normalization = \frac{Overlap}{Chance}$$

Electrophysiology

Ex-vivo acute brain-slice preparation: Brain slices were produced following our previously documented protocols.[62,63] Briefly, rats (p28-p32) were anesthetized with isoflurane, decapitated, and the brain was swiftly dissected out in ice cold carbogenated (95% O2, 5% CO2) standard ACSF (in mM: 126 NaCl, 25 NaHCO3, 3 KCl, 2 CaCl2, 2 MgSO4, 1 NaH2PO4, 0.5 Na-Ascorbate, osmolarity adjusted to 310-315 mOsm with dextrose, pH 7.35). Coronal brain slices (300 μm) containing GC were obtained from both hemispheres of each animal using a vibratome (Leica VT1000). The slices were immediately transferred to a warm (34°C) chamber filled with a continuously carbogenated 'protective recovery' choline-based solution[64] (in mM: 110 Choline-Cl, 25 NaHCO3, 11.6 Na-Ascorbate, 7 MgCl2, 3.1 Na-Pyruvate, 2.5 KCl, 1.25 NaH2PO4, and 0.5 CaCl2, osmolarity 310-315 mOsm, pH 7.35) for 10 minutes, then transferred back to warm (34°C)

carbogenated standard ACSF and incubated another 45 minutes. Brain slices were used for electrophysiology experiments between 1 – 7 hours post-slicing.

Whole-cell recording: Slices were visualized on an Olympus upright epifluorescence microscope using a 10× air (0.13 numerical aperture) and 40× water-immersion objective (0.8 numerical aperture) with infrared-differential interference contrast optics and an infrared CCD camera. Gustatory cortex was identified in acute slices using the shape and morphology of the corpus callosum, piriform cortex and the lateral ventricle as a reference. The borders of GC were determined by comparing the aforementioned landmarks in slice to the Paxinos and Watson rat brain atlas. Pyramidal neurons from superficial and deep layers of agranular and dysgranular GC were visually targeted and identified by the presence of an apical dendrite and teardrop shaped soma. In experiments involving the expression of a viral construct, fluorophore expression was used to visually target pyramidal neurons. Virus expression was consistent across layers and encompassed both dysgranular and agranular regions of GC. Pyramidal morphology was confirmed by post-hoc reconstruction of biocytin fills. Borosilicate glass recording pipettes were pulled using a Sutter P-97 micropipette puller, with acceptable tip resistances ranging from 3 to 6 MΩ. Inclusion criteria for neurons included V_m, R_{in}, and R_s cut-offs as appropriate for experiment type and internal solution. All recordings were performed on submerged slices, continuously perfused with carbogenated 35°C recording solution. Data were low-pass filtered at 10 kHz and acquired at 10 kHz with Axopatch 700B amplifiers and CV-7B headstages (Molecular Devices, Sunnyvale CA). Data were acquired using WaveSurfer v0.953 (Janelia Research Campus), and all post-hoc data analysis was performed using in-house scripts written in MATLAB (Mathworks, Natick MA).

mEPSC recordings: When recording mEPSCs, Cs+ Methanesulfonate-based internal recording solution was used. This Cs+ internal was modified from a previous study,[65] and contained (in mM) 115 Cs-Methanesulfonate, 10 HEPES, 10 BAPTÀ4Cs, 5.37 Biocytin, 2 QX314 Cl, 1.5 MgCl2, 1 EGTA, 10 Na2-Phosphocreatine, 4 ATP-Mg, and 0.3 GTP-Na, with sucrose added to bring osmolarity to 295 mOsm, and CsOH added to bring pH to 7.35.

For these recordings, pyramidal neurons were voltage clamped to −70 mV in standard ACSF containing a drug cocktail of TTX (0.2 μM), APV (50 μM), PTX (25 μM). Traces of 10 seconds were acquired over a period of ~10-15 minutes allowing for the cell to fill for later morphological verification. Neurons were excluded from analysis if Rs > 25 MΩ.

mEPSC analysis: To reliably detect mEPSC events and limit selection bias, we used in-house software that employs a semi-automated template-based detection method.[62,63] Event inclusion criteria included amplitudes greater than 5 pA and rise times less than 3 ms. The resulting events detected by our software were visually assessed for inclusion/exclusion. Our average manual exclusion rate across all experiments was ~9% of events detected. Additionally, the automated detection method missed, on average, ~6% of events, that were manually included. The experimenter was blinded to experimental condition and treatment until after the analysis was complete.

I-Clamp recordings: For I-clamp recordings, a K-gluconate internal recording solution was used. This internal contained (in mM) 100 K-gluconate, 10 KCl, 10 HEPES, 5.37 biocytin, 10 Na2-phosphocreatine, 4 Mg-ATP, and 0.3 Na-GTP, with sucrose added to bring osmolarity to 295 mOsm and KOH added to bring pH to 7.35. Pyramidal neurons in superficial and deep layers of GC expressing inhibitory DREADDS + mCherry were targeted for whole cell recording. The slices were continuously perfused with standard ACSF containing a drug cocktail of APV (50 μM), PTX (25 μM), and DNQX (25 μM). A series of 20 5s traces were recorded; on odd numbered traces input resistance was assessed using a −100 pA, 500 ms DC current injection, while on even numbered traces DC current steps of varying amplitude (−60 to 300 pA) were given to assess firing rate as a function of injected current (FI curves). The V_r and FI curves of hM4D(Gi)$^+$ neurons were assessed before and after perfusion of the exogenous DREADD agonist, CNO (1 μM).

I-Clamp analysis: Changes in input resistance pre and post CNO treatment were calculated using Ohm's Law. Changes in V_r were quantified by analyzing the average resting membrane potential during the 1st minute and 10th minute of the CNO wash. Lastly, action potentials were detected using a custom Matlab script. The results of the spike detection function were visually assessed. Neurons were excluded if Rs > 25 MΩ or V_r > −50 mV.

Biocytin reconstruction: After recording, slices were incubated in cold 4% PFA for two days. Following fixation slices were stained as described above. Biocytin fills were recovered by counterstaining with AlexaFluor streptavidin (ThermoFisher). Images were acquired using the Leica SP5 Laser Scanning Confocal Microscope.

Chemogenetic induction of synaptic scaling: Acute brain slices were prepared as described above, with the exception that TTX was included in the standard ACSF used for slicing and incubation. This was done to prevent any plasticity induction that might occur during release from CNO inhibition in slices rendered hyperexcitable due to chronic inhibition. Pyramidal neurons in superficial and deep layers of GC expressing mCherry were targeted for whole-cell patching and mEPSC recording as described above. For experiments involving the co-injection of hM4D(Gi) and the GluA2-Ctail, cells targeted for recording were confirmed to be expressing both mCherry and GFP post-hoc through immunostaining of cells using antibodies described in the immunohistochemistry section.

Recording from conditioning-active ensemble: Slices were collected exactly 24-hours post conditioning using the methods described above. mEPSCs were recorded using the method described above. For recording, fluorescent RAM$^+$ (tdTomato$^+$) cells were targeted in both superficial and deep layers, where expression was equally robust. For experiments involving the co-injection of RAM and the GluA2-Ctail, cells targeted for recording were confirmed to be expressing both tdTomato and GFP post-hoc through immunostaining of the cells using antibodies described in the immunohistochemistry section.

QUANTIFICATION AND STATISTICAL ANALYSIS

For all experiments including behavior, electrophysiology and imaging, individual experimental distributions were tested for normality using the Anderson-Darling test. If all

experimental conditions passed the normality test, a t-test, paired t-test, or one-way ANOVA were used where appropriate. Significant ANOVA tests were followed by Tukey-Kramer post hoc comparisons. If one or more conditions failed to pass the normality test, a Wilcoxon rank sum or Kruskal-Wallis were used as appropriate. Significant Kruskal-Wallis tests were followed by Bonferroni post hoc comparisons. Differences between cumulative distributions were tested using a two-sample Kolmogorov-Smirnov corrected for multiple comparisons. Results of all statistical tests can be found in the figure legends. For behavior experiments n = number of animals, while for electrophysiology experiments n = number of cells; these values are given in the figure legends. Electrophysiological data were collected from at least 4 animals for each condition. Scatter plots were generated using a publicly available MATLAB code.[66]

Supplementary Material

Refer to Web version on PubMed Central for supplementary material.

ACKNOWLEDGMENTS.

We thank Edwin Zhang for assistance with behavioral experiments and histology, and Brian Cary for help with data analysis. Supported by NIH grants 1 F31 NS108506-01 (RR), R35NS111562 (GGT), and R01DC006666 (DBK).

REFERENCES

1. Hebb DO (1949). The organization of behavior: A neuropsychological theory. New York: John Wiley and Sons, Inc.
2. Bliss TV, and Lomo T (1973). Long-lasting potentiation of synaptic transmission in the dentate area of the anaesthetized rabbit following stimulation of the perforant path. J. Physiol. 232, 331–356. [PubMed: 4727084]
3. Nicoll RA (2017). A Brief History of Long-Term Potentiation. Neuron 93, 281–290. [PubMed: 28103477]
4. Miller KD, and MacKay DJC (1994). The Role of Constraints in Hebbian Learning. Neural Comput. 6, 100–126.
5. Abbott LF, and Nelson SB (2000). Synaptic plasticity: taming the beast. Nat. Neurosci. 3, 1178–1183. [PubMed: 11127835]
6. Tetzlaff C, Kolodziejski C, Timme M, Tsodyks M, and Wörgötter F (2013). Synaptic Scaling Enables Dynamically Distinct Short- and Long-Term Memory Formation. PLOS Comput. Biol. 9, e1003307. [PubMed: 24204240]
7. Zenke F, and Gerstner W (2017). Hebbian plasticity requires compensatory processes on multiple timescales. Philos. Trans. R. Soc. Lond. B. Biol. Sci. 372, 20160259. [PubMed: 28093557]
8. Auth JM, Nachstedt T, and Tetzlaff C (2020). The Interplay of Synaptic Plasticity and Scaling Enables Self-Organized Formation and Allocation of Multiple Memory Representations. Front. Neural Circuits 14, 541728. [PubMed: 33117130]
9. Turrigiano GG, Leslie KR, Desai NS, Rutherford LC, and Nelson SB (1998). Activity-dependent scaling of quantal amplitude in neocortical neurons. Nature 391, 892–896. [PubMed: 9495341]
10. Turrigiano GG (2017). The dialectic of Hebb and homeostasis. Philos. Trans. R. Soc. Lond. B. Biol. Sci. 372, 20160258. [PubMed: 28093556]
11. Turrigiano GG, and Nelson SB (2004). Homeostatic plasticity in the developing nervous system. Nat. Rev. Neurosci. 5, 97–107. [PubMed: 14735113]
12. Turrigiano GG (2008). The self-tuning neuron: synaptic scaling of excitatory synapses. Cell 135, 422–435. [PubMed: 18984155]

13. Ibata K, Sun Q, and Turrigiano GG (2008). Rapid synaptic scaling induced by changes in postsynaptic firing. Neuron 57, 819–826. [PubMed: 18367083]
14. Hengen KB, Lambo ME, Van Hooser SD, Katz DB, and Turrigiano GG (2013). Firing rate homeostasis in visual cortex of freely behaving rodents. Neuron 80, 335–342. [PubMed: 24139038]
15. Garcia J, Kimeldorf DJ, and Koelling RA (1955). Conditioned aversion to saccharin resulting from exposure to gamma radiation. Science 122, 157–158. [PubMed: 14396377]
16. Bures J, Bermudez-Rattoni F, and Yamamoto T (1998). Conditioned Taste Aversion: Memory of a Special Kind. Oxford Psychology Series 31.
17. Escobar ML, Chao V, and Bermddez-Rattoni F (1998). In vivo long-term potentiation in the insular cortex: NMDA receptor dependence. Brain Res. 779, 314–319. [PubMed: 9473708]
18. Rodríguez-Durán LF, Castillo DV, Moguel-González M, and Escobar ML (2011). Conditioned taste aversion modifies persistently the subsequent induction of neocortical long-term potentiation in vivo. Neurobiol. Learn. Mem. 95, 519–526. [PubMed: 21440652]
19. Haley MS, Bruno S, Fontanini A, and Maffei A (2020). LTD at amygdalocortical synapses as a novel mechanism for hedonic learning. eLife 9, e55175. [PubMed: 33169666]
20. Yiannakas A, and Rosenblum K (2017). The Insula and Taste Learning. Front. Mol. Neurosci. 10, 335. [PubMed: 29163022]
21. Welzl H, D'Adamo P, and Lipp H-P (2001). Conditioned taste aversion as a learning and memory paradigm. Behav. Brain Res. 125, 205–213. [PubMed: 11682112]
22. Domjan M (1975). Poison-induced neophobia in rats: Role of stimulus generalization of conditioned taste aversions. Anim. Learn. Behav. 3, 205–211.
23. Chotro MG, and Alonso G (1999). Effects of stimulus preexposure on the generalization of conditioned taste aversions in infant rats. Dev. Psychobiol. 35, 304–317. [PubMed: 10573570]
24. Grobe CL, and Spector AC (2008). Constructing quality profiles for taste compounds in rats: a novel paradigm. Physiol. Behav. 95, 413–424. [PubMed: 18664369]
25. Nachman M, and Ashe JH (1973). Learned taste aversions in rats as a function of dosage, concentration, and route of administration of LiCl. Physiol. Behav. 10, 73–78. [PubMed: 4697023]
26. Berman DE, and Dudai Y (2001). Memory extinction, learning anew, and learning the new: dissociations in the molecular machinery of learning in cortex. Science 291, 2417–2419. [PubMed: 11264539]
27. Hadamitzky M, Bösche K, Engler A, Schedlowski M, and Engler H (2015). Extinction of conditioned taste aversion is related to the aversion strength and associated with c-fos expression in the insular cortex. Neuroscience 303, 34–41. [PubMed: 26126924]
28. Lambo ME, and Turrigiano GG (2013). Synaptic and intrinsic homeostatic mechanisms cooperate to increase L2/3 pyramidal neuron excitability during a late phase of critical period plasticity. J. Neurosci. 33, 8810–8819. [PubMed: 23678123]
29. Gainey MA, and Feldman DE (2017). Multiple shared mechanisms for homeostatic plasticity in rodent somatosensory and visual cortex. Philos. Trans. R. Soc. Lond. B. Biol. Sci. 372, 20160157. [PubMed: 28093551]
30. Teichert M, Liebmann L, Hübner CA, and Bolz J (2017). Homeostatic plasticity and synaptic scaling in the adult mouse auditory cortex. Sci. Rep. 7, 17423. [PubMed: 29234064]
31. Roth BL (2016). DREADDs for Neuroscientists. Neuron 89, 683–694. [PubMed: 26889809]
32. Torrado Pacheco A, Bottorff J, Gao Y, and Turrigiano GG (2021). Sleep Promotes Downward Firing Rate Homeostasis. Neuron. 109, 530–544.e6. [PubMed: 33232655]
33. Gainey MA, Hurvitz-Wolff JR, Lambo ME, and Turrigiano GG (2009). Synaptic scaling requires the GluR2 subunit of the AMPA receptor. J. Neurosci. 29, 6479–6489. [PubMed: 19458219]
34. Goold CP, and Nicoll RA (2010). Single-cell optogenetic excitation drives homeostatic synaptic depression. Neuron 68, 512–528. [PubMed: 21040851]
35. Ancona Esselmann SG, Díaz-Alonso J, Levy JM, Bemben MA, and Nicoll RA (2017). Synaptic homeostasis requires the membrane-proximal carboxy tail of GluA2. Proc. Natl. Acad. Sci. U. S. A. 114, 13266–13271. [PubMed: 29180434]

36. Sun Q, and Turrigiano GG (2011). PSD-95 and PSD-93 Play Critical But Distinct Roles in Synaptic Scaling Up and Down. J. Neurosci. 31, 6800–6808. [PubMed: 21543610]
37. Hayashi T, and Huganir RL (2004). Tyrosine phosphorylation and regulation of the AMPA receptor by SRC family tyrosine kinases. J. Neurosci. 24, 6152–6160. [PubMed: 15240807]
38. Gainey MA, Tatavarty V, Nahmani M, Lin H, and Turrigiano GG (2015). Activity-dependent synaptic GRIP1 accumulation drives synaptic scaling up in response to action potential blockade. Proc. Natl. Acad. Sci. U. S. A. 112, E3590–3599. [PubMed: 26109571]
39. Yaguchi M, Ohashi Y, Tsubota T, Sato A, Koyano KW, Wang N, and Miyashita Y (2013). Characterization of the Properties of Seven Promoters in the Motor Cortex of Rats and Monkeys After Lentiviral Vector-Mediated Gene Transfer. Hum. Gene Ther. Methods 24, 333–344. [PubMed: 23964981]
40. Josselyn SA, and Tonegawa S (2020). Memory engrams: Recalling the past and imagining the future. Science 367, eaaw4325. [PubMed: 31896692]
41. SØrensen AT, Cooper YA, Baratta MV, Weng F-J, Zhang Y, Ramamoorthi K, Fropf R, LaVerriere E, Xue J, Young A, et al. (2016). A robust activity marking system for exploring active neuronal ensembles. eLife 5, e13918. [PubMed: 27661450]
42. Han J-H, Kushner SA, Yiu AP, Cole CJ, Matynia A, Brown RA, Neve RL, Guzowski JF, Silva AJ, and Josselyn SA (2007). Neuronal Competition and Selection During Memory Formation. Science 316, 457–460. [PubMed: 17446403]
43. Morrison DJ, Rashid AJ, Yiu AP, Yan C, Frankland PW, and Josselyn SA (2016). Parvalbumin interneurons constrain the size of the lateral amygdala engram. Neurobiol. Learn. Mem. 135, 91–99. [PubMed: 27422019]
44. Espinosa JS, and Stryker MP (2012). Development and plasticity of the primary visual cortex. Neuron 75, 230–249. [PubMed: 22841309]
45. Lee KJ, Lee Y, Rozeboom A, Lee J-Y, Udagawa N, Hoe H-S, and Pak DTS (2011). Requirement for Plk2 in orchestrated ras and rap signaling, homeostatic structural plasticity, and memory. Neuron 69, 957–973. [PubMed: 21382555]
46. Diering GH, Nirujogi RS, Roth RH, Worley PF, Pandey A, and Huganir RL (2017). Homer1a drives homeostatic scaling-down of excitatory synapses during sleep. Science 355, 511–515. [PubMed: 28154077]
47. Ahmadian G, Ju W, Liu L, Wyszynski M, Lee SH, Dunah AW, Taghibiglou C, Wang Y, Lu J, Wong TP, et al. (2004). Tyrosine phosphorylation of GluR2 is required for insulin-stimulated AMPA receptor endocytosis and LTD. EMBO J. 23, 1040–1050. [PubMed: 14976558]
48. Fox CJ, Russell K, Titterness AK, Wang YT, and Christie BR (2007). Tyrosine phosphorylation of the GluR2 subunit is required for long-term depression of synaptic efficacy in young animals in vivo. Hippocampus 17, 600–605. [PubMed: 17534972]
49. Li W-G, Liu M-G, Deng S, Liu Y-M, Shang L, Ding J, Hsu T-T, Jiang Q, Li Y, Li F, et al. (2016). ASIC1a regulates insular long-term depression and is required for the extinction of conditioned taste aversion. Nat. Commun. 7, 13770. [PubMed: 27924869]
50. Migues PV, Liu L, Archbold GEB, Einarsson EÖ, Wong J, Bonasia K, Ko SH, Wang YT, and Hardt O (2016). Blocking Synaptic Removal of GluA2-Containing AMPA Receptors Prevents the Natural Forgetting of Long-Term Memories. J. Neurosci. 36, 3481–3494. [PubMed: 27013677]
51. Awasthi A, Ramachandran B, Ahmed S, Benito E, Shinoda Y, Nitzan N, Heukamp A, Rannio S, Martens H, Barth J, et al. (2019). Synaptotagmin-3 drives AMPA receptor endocytosis, depression of synapse strength, and forgetting. Science 363, eaav1483. [PubMed: 30545844]
52. Chowdhury D, Turner M, Patriarchi T, Hergarden AC, Anderson D, Zhang Y, Sun J, Chen C-Y, Ames JB, and Hell JW (2018). Ca2+/calmodulin binding to PSD-95 mediates homeostatic synaptic scaling down. EMBO J. 37, 122–138. [PubMed: 29118000]
53. Xu W, Schlüter OM, Steiner P, Czervionke BL, Sabatini B, and Malenka RC (2008). Molecular dissociation of the role of PSD-95 in regulating synaptic strength and LTD. Neuron 57, 248–262. [PubMed: 18215622]
54. Bhattacharyya S, Biou V, Xu W, Schlüter O, and Malenka RC (2009). A critical role for PSD-95/AKAP interactions in endocytosis of synaptic AMPA receptors. Nat. Neurosci. 12, 172–181. [PubMed: 19169250]

55. Sun X, Bernstein MJ, Meng M, Rao S, Sørensen AT, Yao L, Zhang X, Anikeeva PO, and Lin Y (2020). Functionally Distinct Neuronal Ensembles within the Memory Engram. Cell 181, 410–423.e17. [PubMed: 32187527]
56. Rao-Ruiz P, Yu J, Kushner SA, and Josselyn SA (2019). Neuronal competition: microcircuit mechanisms define the sparsity of the engram. Curr. Opin. Neurobiol. 54, 163–170. [PubMed: 30423499]
57. Lopresto D, Schipper P, and Homberg JR (2016). Neural circuits and mechanisms involved in fear generalization: Implications for the pathophysiology and treatment of posttraumatic stress disorder. Neurosci. Biobehav. Rev. 60, 31–42. [PubMed: 26519776]
58. Lis S, Thome J, Kleindienst N, Mueller-Engelmann M, Steil R, Priebe K, Schmahl C, Hermans D, and Bohus M (2020). Generalization of fear in post-traumatic stress disorder. Psychophysiology 57, e13422. [PubMed: 31206738]
59. Flores VL, Moran A, Bernstein M, and Katz DB (2016). Preexposure to salty and sour taste enhances conditioned taste aversion to novel sucrose. Learn. Mem. 23, 221–228. [PubMed: 27084929]
60. Paxinos G, and Watson C (2013). The Rat Brain in Stereotaxic Coordinates - 7th Edition. Academic Press.
61. Khalaf O, Resch S, Dixsaut L, Gorden V, Glauser L, and Graff J (2018). Reactivation of recall-induced neurons contributes to remote fear memory attenuation. Science 360, 1239–1242. [PubMed: 29903974]
62. Miska NJ, Richter LM, Cary BA, Gjorgjieva J, and Turrigiano GG (2018). Sensory experience inversely regulates feedforward and feedback excitation-inhibition ratio in rodent visual cortex. eLife 7, e38846. [PubMed: 30311905]
63. Cary BA, and Turrigiano GG (2019). Stability of cortical synapses across sleep and wake. bioRxiv, 829234.
64. Ting JT, Daigle TL, Chen Q, and Feng G (2014). Acute brain slice methods for adult and aging animals: application of targeted patch clamp analysis and optogenetics. Methods Mol. Biol. 1183, 221–242. [PubMed: 25023312]
65. Xue M, Atallah BV, and Scanziani M (2014). Equalizing excitation-inhibition ratios across visual cortical neurons. Nature 511, 596–600. [PubMed: 25043046]
66. Ramirez ML (2020). UnivarScatter (https://github.com/manulera/UnivarScatter),GitHub.

HIGHLIGHT

- The specificity of Conditioned Taste Aversion (CTA) memory emerges slowly
- Gustatory cortex (GC) neurons express homeostatic synaptic scaling
- CTA-active neurons in GC scale down synaptic weights as memory specificity emerges
- Blocking synaptic downscaling in GC prevents the emergence of memory specificity

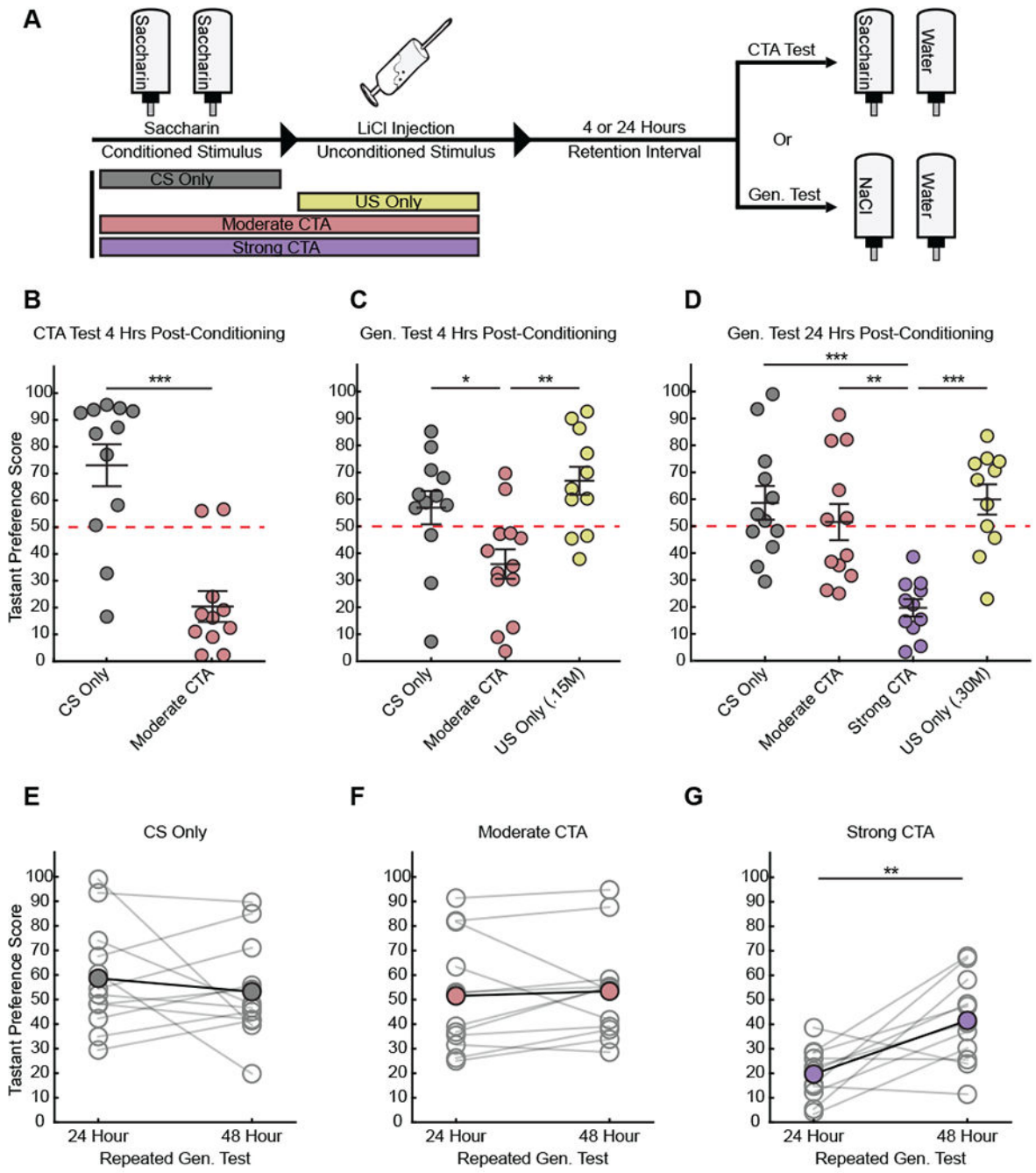

Figure 1 |. Conditioned Taste Aversion (CTA) memory specificity emerges over a timescale of hours.

A) Two-bottle CTA learning paradigm; tastant preference score [(total tastant/total consumed) • 100] were calculated for CTA acquisition (CTA test) or for generalized aversion (Gen. Test) at either 4- or 24-hours post-conditioning. **B)** CTA test; preference for saccharin tested 4 hours after Moderate CTA conditioning (CS Only, n = 12; MCTA, n = 11; Wilcoxon rank-sum test, p = 0.0005; error bars represent SEM). **C)** Gen. test; preference for NaCl tested 4 hours after Moderate CTA conditioning (CS Only, n = 12; MCTA, n = 13; US

Only (.15 M LiCl), n = 11; one-way ANOVA, p = 0.0014; Tukey-Kramer post-hoc test, CS Only vs MCTA p = 0.0319, CS Only vs US Only p = 0.4401, US Only vs MCTA p = 0.0012). **D)** Gen. test; preference for NaCl tested 24 hours after Moderate or Strong CTA conditioning (CS Only, n = 12; MCTA, n = 12; SCTA, n = 11; US Only (.30 M LiCl), n = 11; one-way ANOVA, p = 0.00002; Tukey-Kramer post-hoc test, CS Only vs MCTA p = 0.8029, CS Only vs SCTA p = 0.0001, CS Only vs US Only p = 0.9986, MCTA vs SCTA p = 0.0016, MCTA vs US Only p = 0.7272, SCTA vs US Only p = 0.0001). **E-G)** Gen. test; preference for salt tested 24- & 48-hours post-conditioning (CS Only paired t-test, p = 0.4572; MCTA paired t-test, p = 0.6441; SCTA paired t-test, p = 0.0073). For behavior data here and below, each point represents an individual animal, and the mean and SEM are indicated by line and error bars. Dashed red line indicates no preference. See also Figure S1 and S2.

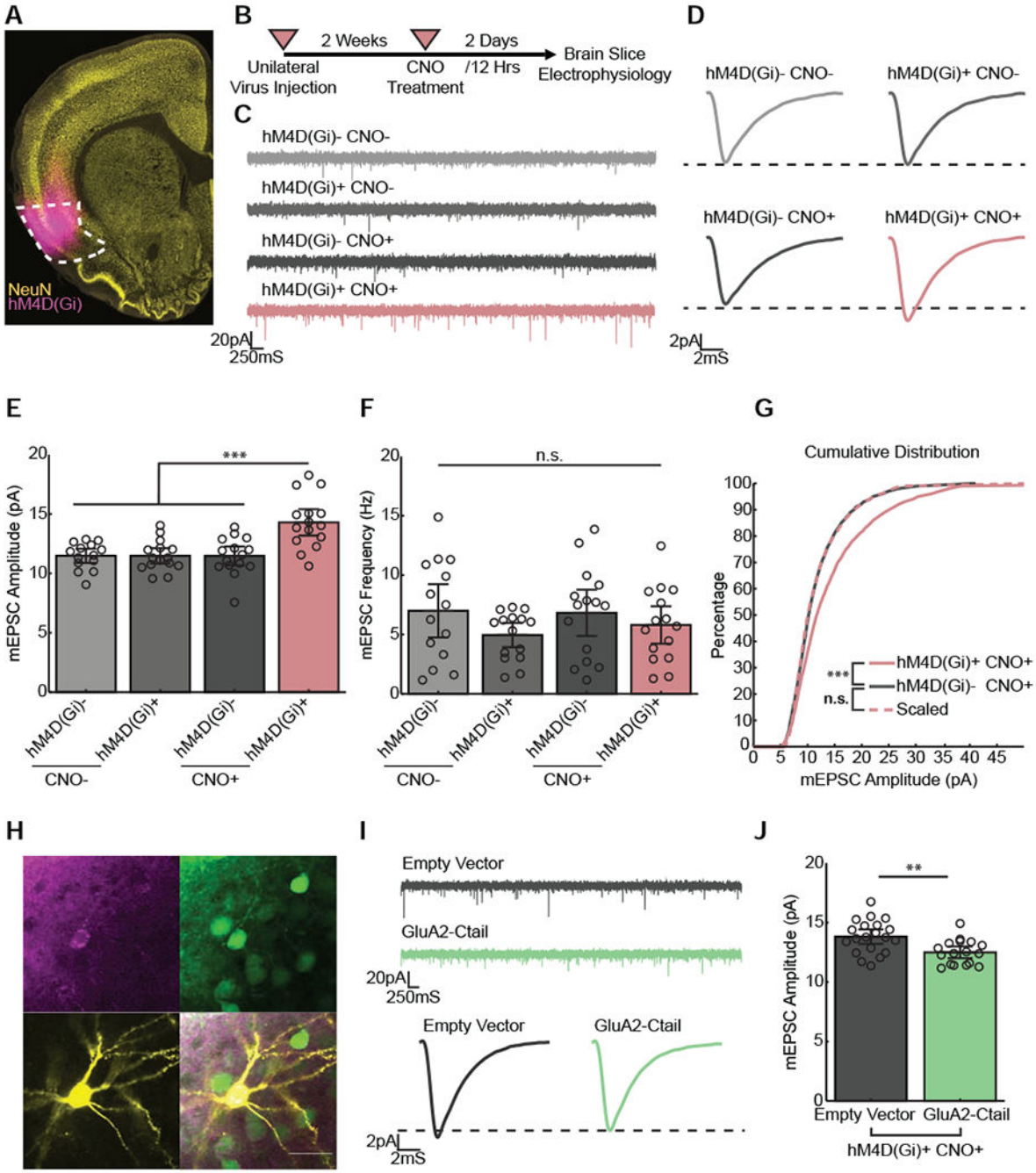

Figure 2 |. Neurons in the gustatory cortex express homeostatic synaptic scaling.

A) Coronal brain slice containing the gustatory cortex (outlined in white), showing neurons expressing the inhibitory DREADDS hM4D(Gi) (magenta signal). **B)** Experimental protocol. **C)** Representative mEPSC recordings. **D)** Average mEPSC waveform for each condition, black dashed line is aligned to $hM4D(Gi)^{-}$ CNO^{-} waveform peak. **E)** Cell-average mEPSC amplitudes ($hM4D(Gi)^{-}$ CNO^{-}, n = 14; $hM4D(Gi)^{+}$ CNO“ n = 15; $hM4D(Gi)^{-}$ CNO^{+}, n = 15; $hM4D(Gi)^{+}$ CNO^{+}, n = 15; one-way ANOVA, p = 5.8849e-06; Tukey-Kramer post-hoc test, $hM4D(Gi)^{+}$ CNO^{+} vs $hM4D(Gi)^{-}$ CNO^{+} p = 0.0001,

hM4D(Gi)$^+$ CNO$^+$ vs hM4D(Gi)$^+$ CNO$^-$ p = 0.0001, hM4D(Gi)$^+$ CNO$^+$ vs hM4D(Gi)$^-$ CNO$^-$ p = 0.0001; error bars represent 95% confidence interval, CI). **F)** Cell-average mEPSC event frequency (one-way ANOVA, p = 0.3377). **G)** Cumulative histogram of mEPSC amplitudes sampled from hM4D(Gi)$^+$ CNO$^+$ and hM4D(Gi)$^-$ CNO$^+$ conditions. Pink dashed line represents hM4D(Gi)$^+$CNO$^+$ distribution scaled according to the linear function $f(x) = 0.6646x + 2.366$ (two-sample Kolmogorov-Smirnov test; Bonferroni correction $\alpha = 0.025$; hM4D(Gi)$^+$ CNO$^+$ vs hM4D(Gi)$^-$ CNO$^+$, p = 6.2093e-07, Scaled vs hM4D(Gi)$^-$ CNO$^+$, p = 0.5231). **H)** Biocytin fill of a recorded pyramidal cell in GC co-expressing hM4D(Gi) and the GluA2-Ctail (scalebar: 25μM). **I)** Top: representative mEPSC recordings; bottom: average mEPSC waveforms, black dashed line is aligned to GluA2-Ctail waveform peak. **J)** Cell-average mEPSC amplitudes (Empty Vector, n = 20; GluA2-Ctail, n = 17; two-sample t-test, p = 0.0029). For electrophysiological data here and below, each point represents a recorded neuron; the mean and CI are represented by line and error bars. See also Figure S3.

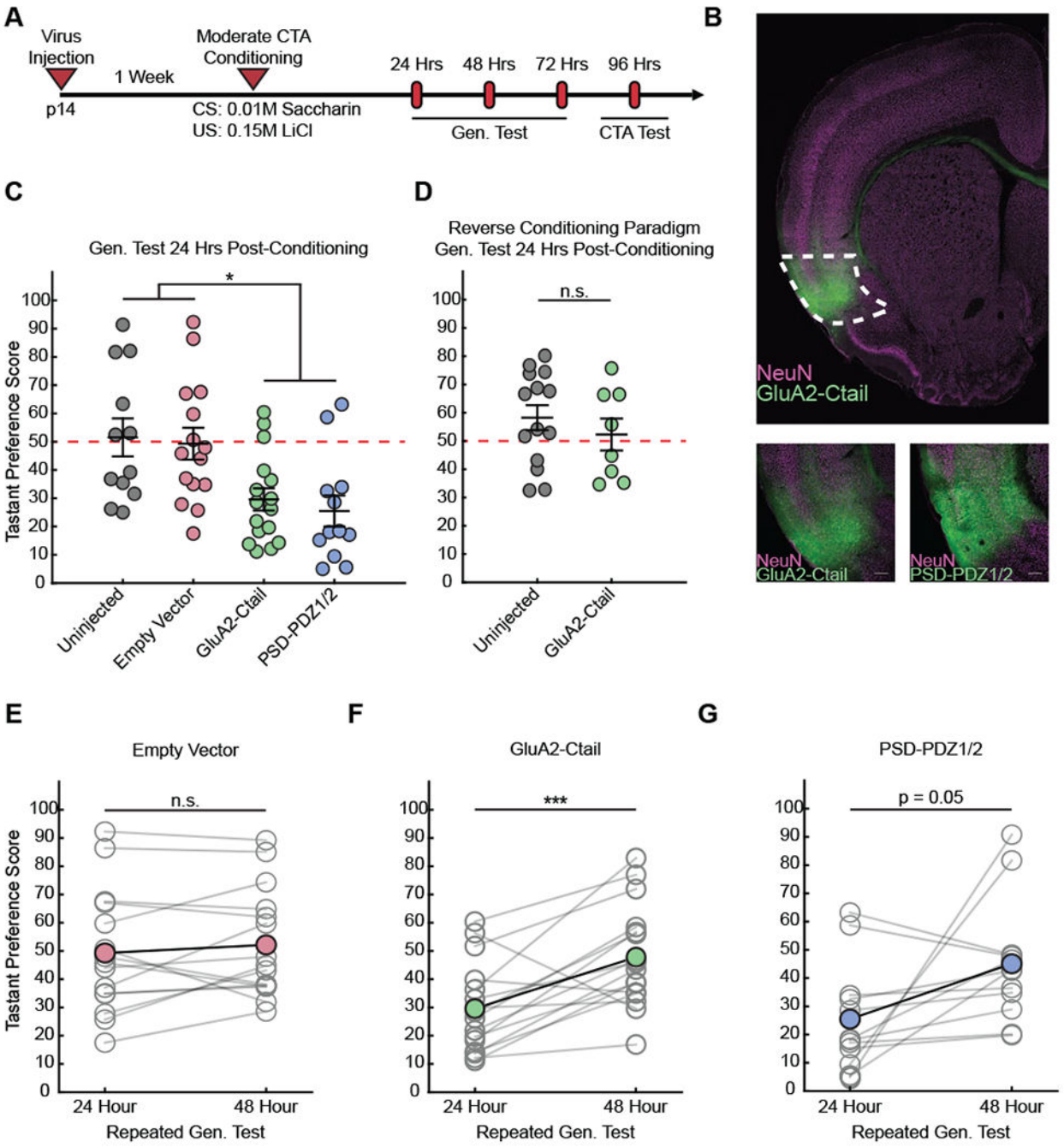

Figure 3 |. Perturbation of synaptic scaling prolongs CTA-induced generalized aversion.

A) Experimental timeline. **B)** Top: representative image depicting expression of the GluA2-Ctail in GC (outlined in white; scalebar: 500 μM). Bottom: zoomed-in images showing expression of the GluA2-Ctail (left) and the PSD-PDZ1/2 fragment (right; scalebar: 500 μM). **C)** Gen. test; preference for NaCl tested 24 hours after Moderate CTA conditioning (Uninjected, n = 12; Empty Vector, n = 15; GluA2-Ctail, n = 16; PSD-PDZ1/2, n = 12; one-way ANOVA, p = 0.0015; Tukey-Kramer post-hoc test, UnInj. vs EV p = 0.9915, UnInj. vs Ctail p = 0.0289, UnInj. vs PSD p =0.0124, EV vs Ctail p = 0.0401, EV vs PSD p = 0.0170,

Ctail vs PSD p = 0.9490; error bars represent SEM). **D)** Gen. test; preference for NaCl tested 24 hours after the unpaired reverse conditioning paradigm (Uninjected, n = 14; GluA2-Ctail, n = 8; two-sample t-test, p = 0.4206). **E-G)** Gen. test; preference for salt tested 24- & 48-hours post-conditioning (Empty Vector paired t-test, p = 0.3596; GluA2-Ctail paired t-test, p = 9.6572e-04; PSD-PDZ1/2 paired t-test, p = 0.0531). See also Figure S4 and S5.

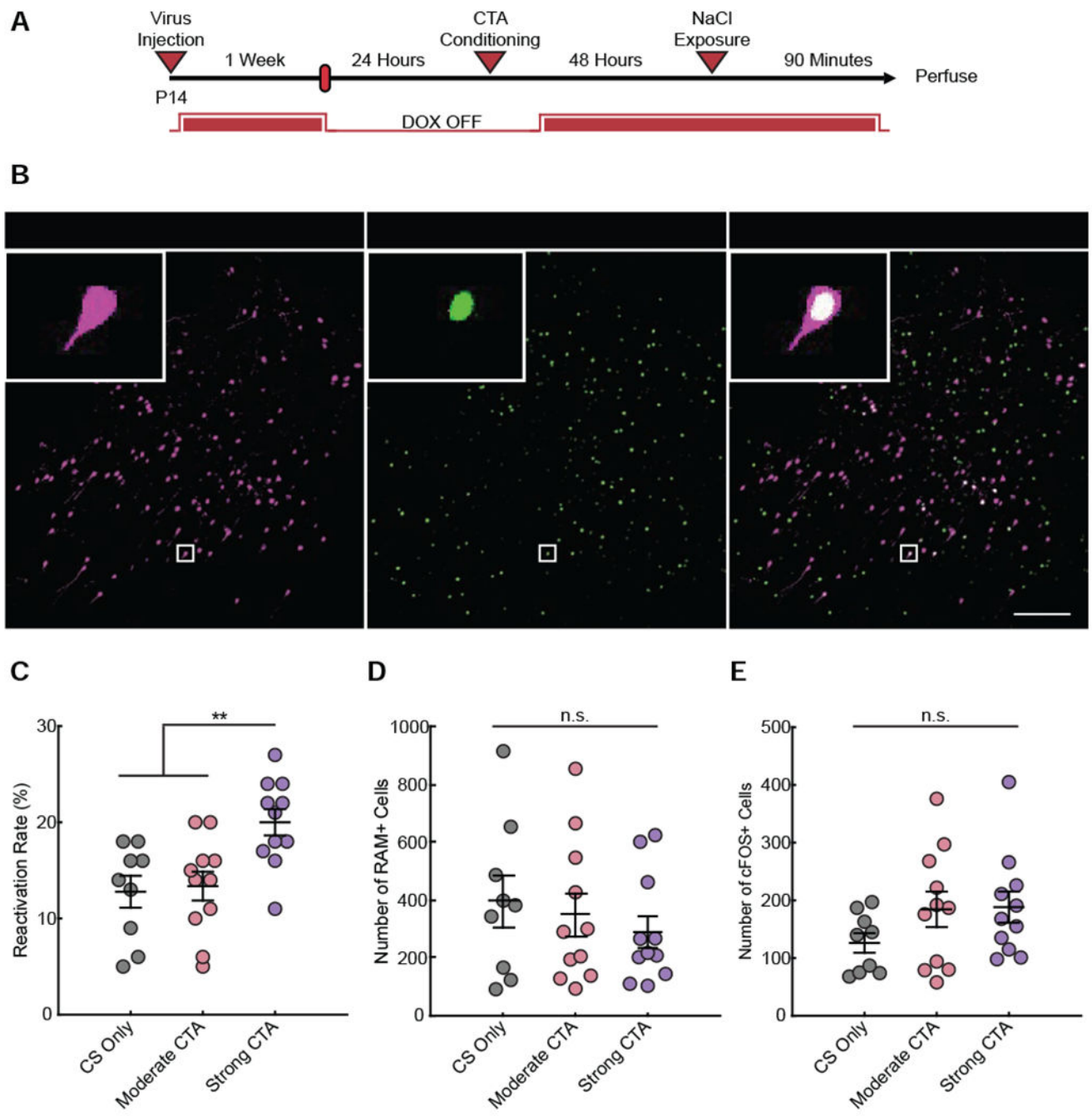

Figure 4 |. Conditioning-active gustatory cortex neuronal ensembles are reactivated during generalized aversion.

A) Experimental paradigm for labeling conditioning-active GC ensembles and their reactivation by the generalized tastant (NaCl). **B)** Representative images showing conditioning-active GC ensembles (RAM^+, left), neurons activated by presentation of NaCl ($c\text{-}FOS^+$, middle), and their overlap ($RAM^+c\text{-}FOS^+$, right; scalebar: 200 μM). **C)** Reactivation rate of conditioning-active neurons ($RAM^+c\text{-}FOS^+/RAM^+$; CS Only, n = 9; MCTA, n = 11; SCTA, n = 11; one-way ANOVA, p = 0.0027; Tukey-Kramer post-hoc test,

CS Only vs MCTA p = 0.9604, CS Only vs SCTA p = 0.0065, MCTA vs SCTA p = 0.0085; error bars represent SEM). **D)** Number of RAM^+ cells (Kruskal-Wallis, p = 0.7598). **E)** Number of c-FOS^+ cells (one-way ANOVA, p = 0.2238). See also Figure S6.

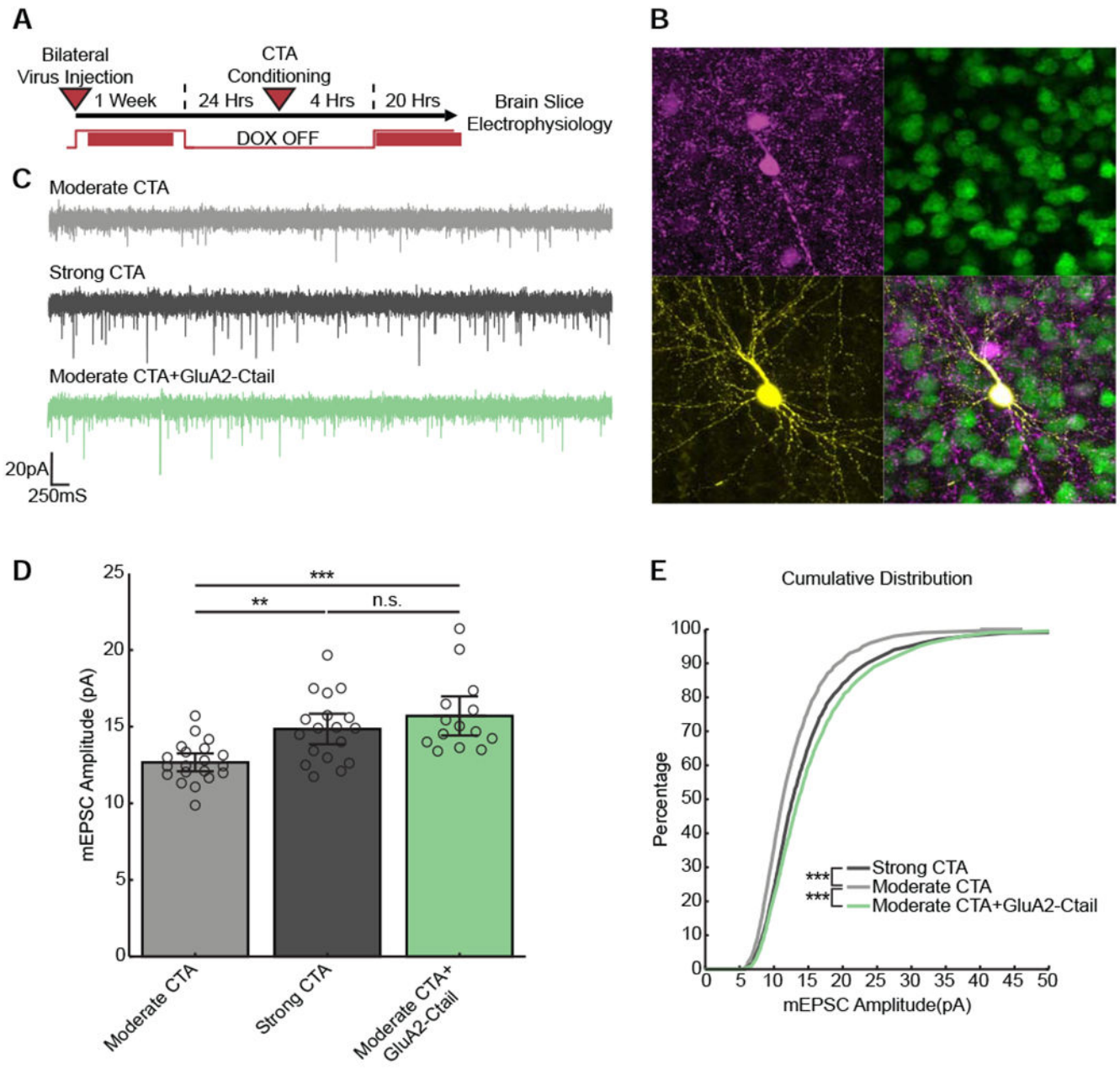

Figure 5 |. Blocking synaptic scaling causes a persistent increase in synaptic strength onto CTA-active neuronal ensembles following CTA conditioning.

A) Experimental timeline. **B)** Biocytin fill of a pyramidal cell in GC expressing RAM (scalebar: 25 μM) **C)** Representative mEPSC recordings. **D)** Cell-average mEPSC amplitudes of RAM^{+} neurons 24 hours after CTA conditioning (Moderate CTA, n = 20; Strong CTA, n = 18; Moderate CTA+GluA2-Ctail, n = 14; one-way ANOVA, p = 1.0568e-04; Tukey-Kramer post-hoc test, Moderate CTA vs Strong CTA p = 0.0037, Moderate CTA vs Moderate CTA+GluA2-Ctail p = 0.0002, Strong CTA vs Moderate CTA +GluA2-Ctail p = 0.4516; error bars represent 95% CI) **E)** Cumulative histogram of mEPSC amplitudes (two-sample Kolmogorov-Smirnov test; Bonferroni correction $\alpha = 0.025$;

Moderate CTA vs Strong CTA p = 1.5833e-06, Moderate CTA vs Moderate CTA+GluA2-Ctail p = 1.0611e-11).

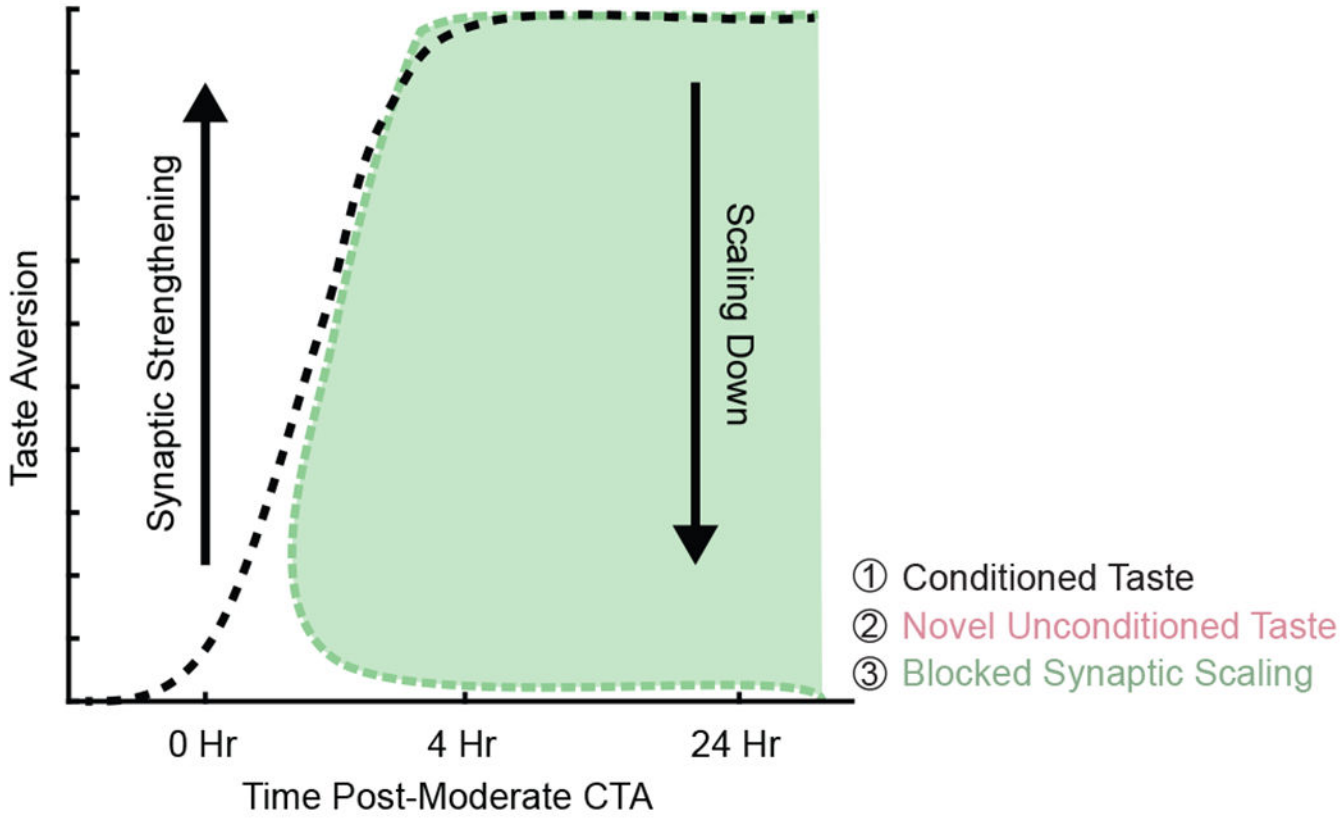

Figure 6 |. Summary of findings.

Our results demonstrate that after Moderate CTA conditioning animals learn an aversion to the conditioned taste (1, black dashed line) and they also exhibit a transient generalized aversion to a novel unconditioned taste (2, magenta solid line). Blocking synaptic scaling (3, green dashed line) prolongs the duration of the generalized aversion and produces a persistent increase in postsynaptic strengths onto CTA-active neuronal ensembles. Together, our data support the hypothesis that homeostatic synaptic scaling within GC shapes the specificity of CTA memory.

KEY RESOURCES TABLE

REAGENT or RESOURCE	SOURCE	IDENTIFIER
Antibodies		
Chicken polyclonal anti-GFP	Aves Labs	GFP-1020; RRID: AB_2307313
Mouse monoclonal anti-NeuN (A60)	Millipore	MAB-377; RRID: AB_2298772
Mouse monoclonal anti-RFP (8E5.G7)	Rockland	200-301-379; RRID: AB_2611063
Rabbit monoclonal anti-c-FOS (9F6)	Cell Signaling Technology	2250; RRID: AB_2247211
Rat monoclonal anti-mCherry (16D7)	Thermo-Fisher	M11217; RRID: AB_2536611
Goat polyclonal anti-chicken Alexa Fluor 488	Thermo-Fisher	A-11039; RRID: AB_142924
Goat polyclonal anti-mouse Alexa Fluor 594	Thermo-Fisher	A-11032; RRID: AB_2534091
Goat polyclonal anti-rat Alexa Fluor 594	Thermo-Fisher	A-11007; RRID: AB_10561522
Goat polyclonal anti-mouse Alexa Fluor 555	Thermo-Fisher	A-21424; RRID: AB_141780
Goat polyclonal anti-rabbit Alexa Fluor 647	Thermo-Fisher	A-21245; RRID: AB_2535813
Streptavidin Alexa Fluor 647	Thermo-Fisher	S-32357
Streptavidin Alexa Fluor 488	Thermo-Fisher	S-11223
Bacterial and Virus Strains		
AAV2/1-CMV-GluA2-CT	Lambo and Turrigiano.[28]	N/A
AAV2/1-CMV-PSD95-PDZ1/2	This manuscript	N/A
AAV2/1-CMV-eGFP3	This manuscript	N/A
AAV9-RAM-d2tTA-TRE-tdTomato	This manuscript	N/A
AAV9-CAMKIIα-hM4D(Gi)-mCherry	This manuscript	N/A
Lentivirus-CAMKIIα-GFP-GluA2-Y876E	This manuscript	N/A
Lentivirus-CAMKIIα-GFP-GluA2-WT	This manuscript	N/A
Chemicals, Peptides, and Recombinant Proteins		
Clozapine N-oxide	Hello Bio	HB6149
Tetrodotoxin	Tocris	1069
DL-APV	Tocris	0105
Picrotoxin	Sigma-Aldrich	P1675-5G
DNQX	Sigma-Aldrich	D0540
Hoechst 33342, Trihydrochloride, Trihydrate	Thermo-Fisher	H3570
Experimental Models: Organisms/Strains		
Timed-pregnant Long-Evans rats	Charles River Laboratories	006L/E
Recombinant DNA		
pAAV-CMV-GluA2-CT	Lambo and Turrigiano[28]	N/A
pAAV-CMV-PSD95-PDZ1/2	This manuscript	N/A
pAAV-CMV-eGFP3	This manuscript	N/A
pAAV-RAM-d2tTA-TRE-tdTomato	This manuscript	N/A
pAAV-RAM-d2tTA-TRE-GFP-WPREpA	Sørensen et al.[41]	Addgene: 84469
pAAV-CAMKIIα-hM4D(Gi)-mCherry	Gift from Bryan Roth	Addgene: 50477

REAGENT or RESOURCE	SOURCE	IDENTIFIER
Lenti-CAMKIIα-GFP-GluA2-Y876E	This manuscript	N/A
Lenti-CAMKIIα-GFP-GluA2-WT	This manuscript	N/A
Software and Algorithms		
ZEN Black acquisition software	Zeiss	https://www.zeiss.com; RRID: SCR_018163
ImageJ/FIJI	FIJI	http://fiji.sc RRID: SCR_002285
MATLAB	Mathworks	https://www.mathworks.com; RRID: SCR_001622
Custom MATLAB scripts	Cary and Turrigiano.[63]	https://github.com/BrianAndCary/papers/tree/master/bcary2020_paper/mini_FI_GUI
Other		
5P00 chow with 40 ppm doxycycline	ScottPharma	5BN7; 1818670-209
5P00 chow with 100 ppm doxycycline	ScottPharma	5BN6; 1818669-209
DAPI-Fluoromount-G mounting medium	SouthernBiotech	0100-20
Fluoromount-G mounting medium	SouthernBiotech	0100-01